Quality Improvement Study

Medicine®

OPEN

The effect of the reconstruction algorithm for the pulmonary nodule detection under the metal artifact caused by a pacemaker

Noriko Kikuchi, MD[a,*], Masahiro Yanagawa, MD, PhD[a], Yukihiro Enchi, RT[b], Akiko Nakayama, MD[a], Yuriko Yoshida, MD[a], Tomo Miyata, MD[a], Akinori Hata, MD, PhD[a], Mitsuko Tsubamoto, MD, PhD[c], Osamu Honda, MD, PhD[c], Noriyuki Tomiyama, MD, PhD[a]

Abstract

The aim was to compare the effects of metal artifacts from a pacemaker on pulmonary nodule detection among computed tomography (CT) images reconstructed using filtered back projection (FBP), single-energy metal artifact reduction (SEMAR), and forward-projected model-based iterative reconstruction solution (FIRST).

Nine simulated nodules were placed inside a chest phantom with a pacemaker. CT images reconstructed using FBP, SEMAR, and FIRST were acquired at low and standard dose, and were evaluated by 2 independent radiologists.

FIRST demonstrated the most significantly improved metal artifact and nodule detection on low dose CT ($P < .0032$), except at 10 mA and 5-mm thickness. At standard-dose CT, SEMAR showed the most significant metal artifact reduction ($P < .00001$). In terms of nodule detection, no significant differences were observed between FIRST and SEMAR ($P = .161$).

With a pacemaker present, FIRST showed the best nodule detection ability at low-dose CT and SEMAR is comparable to FIRST at standard dose CT.

Abbreviations: CT = computed tomography, CTDIvol = CT dose index volume, DLP = dose-length product, ED = effective dose, FBP = filtered back projection, FIRST = forward-projected model-based iterative reconstruction solution, GGN = ground-glass nodule, HU = hounsfield units, MAR = metal artifact reduction, MBIR = model based iterative reconstruction, ROI = region of interest, SD = standard deviation, SEMAR = single-energy metal artifact reduction, SNR = signal-to-noise ratio.

Keywords: metal artefacts, nodule detection, radiation dose, reconstruction technique

1. Introduction

Artifacts are clinically seen on computed tomography (CT). In particular, metal artifacts are very commonly seen in patients with metallic implants such as metallic dental fillings, artificial joints, bone fixation screws, and pacemakers. Metal artifacts are caused by multiple mechanisms, including beam hardening, Compton scatter, and Poisson noise.[1,2] The combination of beam hardening, scatter, and photon starvation produces dark streaks. In addition, motion and undersampling create sharp, thin alternating streaks surrounding metal implants. Smoothly undulating streaks surrounding metal implants are the result of windmill artifacts.[2]

Metal artifacts can be reduced under various technical procedures.[3] Dual-energy CT is useful for reducing these artifacts, but a specific CT scanner and scanning protocol are required. At the single-energy CT reconstruction step, metal-implanting methods or iterative reconstruction algorithms are available to reduce metal artifacts.[4,5] Single-energy metal artifact reduction (SEMAR) is a technique developed by Canon Medical Systems Corporation for 320-detector CT scanners (Aquilion ONE Vision; Canon Medical Systems Corp., Otawara, Tochigi, Japan).[6] The metal components are first segmented from the original image using SEMAR. These data are then forward-projected to identify and correct metal traces on the sinogram. Back projections, tissue classification, and forward projections are then applied to reconstruct the final images.[4,5] The forward-projected model-based iterative reconstruction solution (FIRST) was developed as an iterative method for image reconstructions.[6] Noise is independently reduced in sinograms and image spaces, and full iterative reconstruction results in fewer streak artifacts and improve spatial resolution on sinograms through forward projection jointly using data from the fidelity, optic, system, cone-beam, and statistical noise models.[7]

Editor: YX Sun.

The authors report no conflicts of interest.

The datasets generated during and/or analyzed during the current study are not publicly available, but are available from the corresponding author on reasonable request. All authors don't receive any fundings.

[a] From the Department of Radiology, Osaka University Graduate School of Medicine, Suita-city, [b] Division of Radiology, Department of Medical Technology, Osaka University Hospital, Suita, [c] From the Department of Radiology, Kansai Medical University, Hirakata City, Osaka, Japan.

[*] Correspondence: Noriko Kikuchi, The Department of Radiology, Osaka University Graduate School of Medicine, 2–2 Yamadaoka, Suita-city, Osaka 565–0871, Japan (e-mail: n-kikuchi@radiol.med.osaka-u.ac.jp).

How to cite this article: Kikuchi N, Yanagawa M, Enchi Y, Nakayama A, Yoshida Y, Miyata T, Hata A, Tsubamoto M, Honda O, Tomiyama N. The Effect of the Reconstruction Algorithm for the pulmonary nodule detection under the metal artifact caused by a pacemaker. Medicine 2020;99:24(e20579).

Received: 12 November 2019 / Received in final form: 27 April 2020 / Accepted: 2 May 2020

http://dx.doi.org/10.1097/MD.0000000000020579

One unique feature of FIRST is that even further noise reduction can be achieved through the use of anatomical-based regularization model and adaptive iteration using forward-projected data.[8] The regularization process is to optimize for specific organs (eg, bone, heart, lung, and abdomen) to reduce image noise.[9] FIRST can maintain high spatial resolution even with lower-dose CT.

We hypothesized that metal artifacts from a pacemaker on low- and standard-dose CT images of 5- and 0.5-mm slice thickness may impede pulmonary nodule detection, and this effect might be improved by reconstruction techniques. The purpose of this study was to compare the effects of metal artifacts from a pacemaker on pulmonary nodule detection among low- and standard-dose CT images reconstructed using filtered back projection (FBP), SEMAR, and FIRST.

2. Materials and methods

2.1. Chest CT Phantom and CT Image Acquisition

Approvement by the institutional review board and the requirement for obtaining informed consent were waived because only phantom data were used in this study. A commercially available chest CT phantom (N-1; Kyoto Kagaku, Kyoto, Japan) and simulated nodules were used. The simulated nodules were composed of urethane resin and hydroxyapatite. CT attenuation values for the simulated nodules were –800 Hounsfield units (HU) (ground-glass nodule [GGN] phantom), –630 HU (GGN phantom), and +100 HU (solid nodule phantom), which were provided with the manual from Kyoto Kagaku. Diameters of the simulated nodules were 3, 5, and 10 mm, respectively. As a result, 9 patterns of simulated nodules were prepared. A clinically used pacemaker (Kappa SR701; Medtronic, Minneapolis, MN) was placed on the surface of the left chest wall of the phantom (Fig. 1).

All CT data were obtained using a 320-detector row CT scanner (Aquilion ONE; Canon Medical Systems, Otawara, Japan). The CT protocol was as follows: detector collimation, 0.5 mm; detector pitch, 0.813; gantry rotation period, 0.5; matrix size 512 × 512 pixels; x-ray voltage 120 kV; and 3 tube currents (10, 50, and 300 mA).

The chest phantom with pacemaker was scanned without the nodule. Each of the 9 simulated nodules was then attached to the lung field posterior to the pacemaker. Image data were acquired with the CT scanner. Axial CT images of 5- and 0.5-mm slice thickness were reconstructed with FBP, SEMAR, and FIRST.

2.2. Subjective image analysis

A total of 162 images were obtained, using 9 different simulated nodules, 3 tube currents, 2 slice thicknesses, and 3 reconstruction algorithms (FBP, SEMAR, and FIRST). Two independent radiologists with 9 and 10 years of experience reviewed the 162 images on a 5-megapixel 21-in monochrome liquid-crystal display monitor without prior knowledge of the image acquisition parameters or iterative reconstruction techniques. All images were displayed at a window level of -700 HU and a window width of 1200 HU.

The same 2 radiologists assessed the impact of metal artifacts using a 3-point scale (1, none to 3, severe) and detection of the nodule on a 5-point scale (1, definitely absent to 5, definitely present). If the evaluations were inconsistent between radiologists, another radiologist with 19 years of experience reevaluated the metal artifact or presence of the nodule.

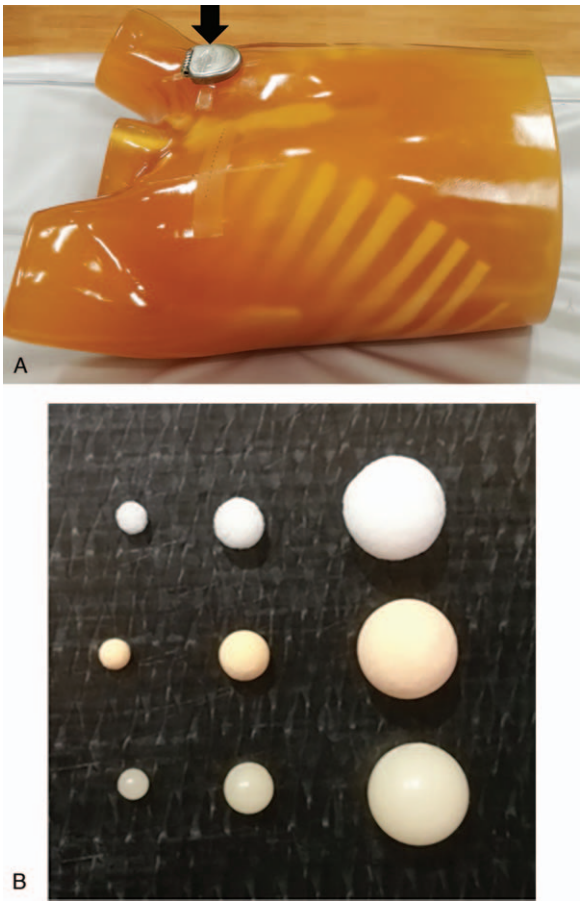

Figure 1. (A) Chest computed tomography (CT) phantom with a pacemaker (arrow). (B) Nine patterns of simulated nodules. The simulated nodules are composed of urethane resin and hydroxyapatite. The CT numbers are –800, –630, and +100 HU. The diameters are 3, 5, and 10 mm. Each of the 9 simulated nodules was attached in the lung field underneath the pacemaker.

2.3. Objective analysis

Quantitative noise measurements were calculated by measuring standard deviation (SD) in a circular region of interest (ROI) defined by an electric cursor, using free software (ImageJ version 1.37 v; NIH, Bethesda, MD; for further information regarding ImageJ software, see http://rsb.info.nih.gov/ij/index.html). ROIs (200 mm^2) were placed in 4 homogeneous parts of an image in the air adjacent to the lung specimen and were confirmed to be in exactly the same location on each image in a series. Average values of SD were analyzed statistically. Signal-to-noise ratio (SNR) in each area with prominent artifacts was measured quantitatively using mean CT values and SDs in a circular ROI (200 mm^2) on a workstation (Figs. 2 and 3). The formula to calculate the SNR was as follows: |mean CT|/SD.

2.4. Statistical analysis

All statistical analyses were performed using commercially available software (MedCalc version 12.3.0.0 statistical software; Frank Schoonjans, Mariakerke, Belgium). Statistical analyses were performed with the Friedman test followed by post-hoc tests. A value of $P < .017$ (0.05/3) using Bonferroni correction was considered significant.

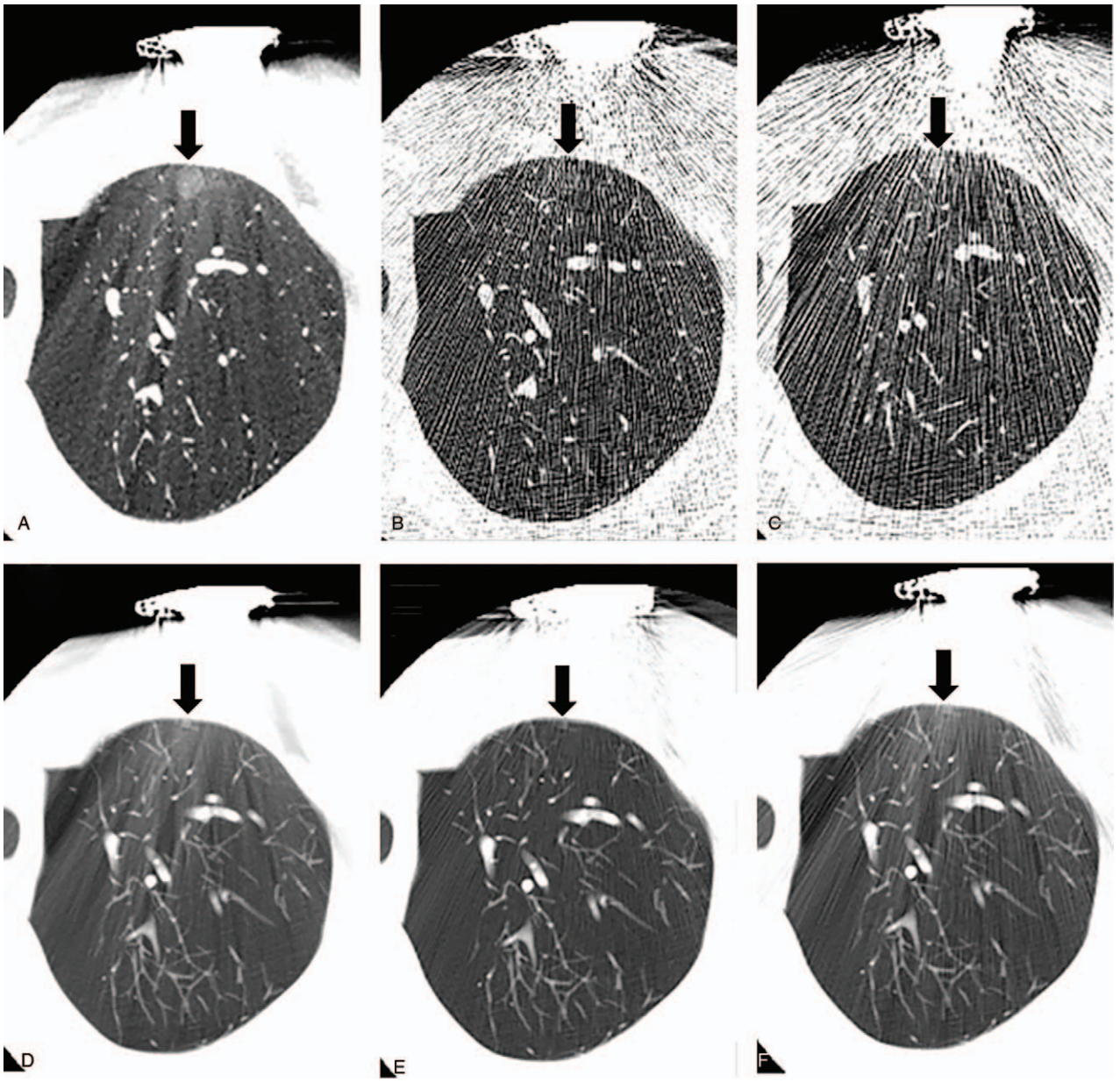

Figure 2. Typical computed tomography (CT) images of nodules underneath a pacemaker. (A–C) at 50 mA dose, a -800 HU and 10 mm nodule with 0.5 mm thickness on FIRST, SEMAR, and FBP respectively (D–F) at 300 mA dose, a -630 HU and 3 mm nodule with 5 mm thickness on FIRST, SEMAR, and FBP. FBP = filtered back projection, FIRST = forward-projected model-based iterative reconstruction solution, SEMAR = single-energy metal artifact reduction.

3. Results

3.1. Radiation doses

Low radiation doses (10, 50 mA) and a standard dose (300 mA) were used in scanning of the chest CT phantom with a pacemaker. The reported radiation dose measurements consist of the CT dose index volume (CTDIvol), dose-length product (DLP), and effective dose (ED), calculated as the product of DLP and the "κ" conversion coefficient (0.014 mSv/[mGy cm]) for chest CT.[10] The CTDIvol, DLP, and ED were: 0.3 mGy, 3.6 mGy cm, and 0.05 mSv, respectively, for 10 mA; 1.7 mGy, 18.2 mGy cm, and 0.25 mSv for 50 mA; and 10.2 mGy, 109.4 mGy cm, and 1.53 mSv for 300 mA. Scan length for calculating DLP was 60 mm, as a range that sufficiently contained each simulated nodule and the pacemaker.

3.2. Metal artifacts

The effects of metal artifacts from the pacemaker at different doses were evaluated. Mean and SD of the metal artifact scores are summarized in Table 1. On low-dose (10 mA or 50 mA) CT images of 5- and 0.5-mm slice thickness, FIRST showed significantly lower scores than FBP or SEMAR. On the contrary, at standard dose (300 mA) CT images of 5- and 0.5-mm slice thickness, SEMAR showed a significantly lower score than FIRST or FBP.

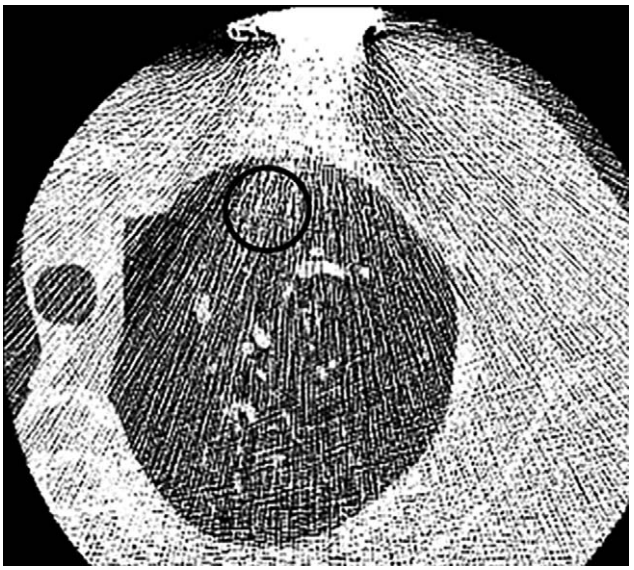

Figure 3. An example of ROI placement for SNR measurement. ROI = region of interest, SNR = signal-to-noise ratio.

3.3. Total nodule detection

Detection of nodules with 9 different patterns was subsequently evaluated. Nodule detection scores are shown in Table 2. On low-dose (50 mA) images of 5-mm slice thickness, FIRST showed significantly higher scores than FBP or SEMAR ($P = .0136$), and even at ultra-low dose (10 mA), FIRST showed this tendency. With a standard-dose CT image of 5-mm slice thickness, scores were in descending order of FIRST, SEMAR, and FBP. On low-dose CT images of 0.5-mm slice thickness, FIRST showed significantly higher scores than FBP or SEMAR (10 mA, $P = .0032$; 50 mA, $P = .0015$), whereas with standard-dose CT images of 0.5-mm slice thickness, both FIRST and SEMAR tended to show higher scores than FBP, but no significant differences were apparent between the three. Representative CT images are shown on Figure 3.

3.4. Nodule detection according to nodule density

Nodule detection scores were stratified by nodule density (Table 3). FIRST showed the best scores under any conditions (nodule density, dose, and image thickness). SEMAR showed scores somewhere between FBP and FIRST; with standard dose, the score was somewhat similar to that of FIRST, whereas with low dose the score was closer to that of FBP. As expected, when nodule density decreased, the nodule detection score decreased (from 100 HU simulating solid nodule to –630 HU simulating GGN and –800 HU simulating GGN). Although little difference was seen between 0.5 and 5 mm thickness with the 100-HU nodule, the detection score decreased on 0.5-mm thickness compared to 5 mm with nodules of -630 HU and -800 HU.

3.5. Nodule detection according to nodule size

Nodule detection scores stratified by nodule size were also analyzed (Table 4). As in the previous analysis, FIRST always

Table 1

Metal artifact score (5 mm/0.5 mm thickness).

Slice thickness	5 mm			0.5 mm		
Radiation dose	10 mA	50 mA	300 mA	10 mA	50 mA	300 mA
FBP	3.0 ± 0.0[*]	3.0 ± 0.0[*]	3.0 ± 0.0[*]	3.0 ± 0.0[*]	3.0 ± 0.0[*]	2.6 ± 0.5[*]
SEMAR	3.0 ± 0.0[†]	2.7 ± 0.5[†]	1.0 ± 0.3[*]	3.0 ± 0.0[†]	2.9 ± 0.3[†]	1.4 ± 0.5[*]
FIRST	2.0 ± 0.0[*,†]	2.0 ± 0.0[*,†]	2.0 ± 0.0[*]	2.0 ± 0.0[*,†]	2.0 ± 0.0[*,†]	2.0 ± 0.0[*]
Group comparison ($P^{\ddagger}$)	.001	.00001	<.00001	.0001	<.00001	<.00001

Data are presented as mean ± standard deviation. Data of the subjective image analysis on metal artifact score (3-point scale: 1, almost absent; 2, mild, diagnosis is possible; 3, severe, nondiagnostic) were statistically analyzed using the Friedman test with a Bonferroni Correction applied for multiple comparisons. FBP = filtered back projection, FIRST = forward projected model-based iterative reconstruction solution, SEMAR = single energy metal artifact reduction.

[*,†]A significant difference presents between the 2 or 3 groups.

[‡] Bonferroni-corrected *P* value.

Table 2

Nodule detection score—all types of nodules included (5 mm/0.5 mm thickness).

Slice thickness	5 mm			0.5 mm		
Radiation dose	10 mA	50 mA	300 mA	10 mA	50 mA	300 mA
FBP	1.9 ± 1.5	2.2 ± 1.7[*]	3.6 ± 1.6	1.4 ± 1.0[*]	2.1 ± 1.5[*]	3.5 ± 1.5
SEMAR	1.9 ± 1.5	3.0 ± 1.8[†]	3.9 ± 1.5	1.5 ± 1.0[†]	2.4 ± 1.5[†]	4.1 ± 1.0
FIRST	2.8 ± 1.6	3.9 ± 1.5[*,†]	4.1 ± 1.5	3.1 ± 1.7[*,†]	4.1 ± 0.9[*,†]	4.4 ± 1.0
Group comparison ($P^{\ddagger}$)	.141	.0136	.161	.0032	.0015	.113

Data are presented as mean ± standard deviation. Data of the subjective image analysis on nodule detection score (5-point scale: 1, definitely absent; 2, probably absent; 3, undeterminable; 4, probably present; 5, definitely present) were statistically analyzed using the Friedman test with a Bonferroni Correction applied for multiple comparisons.

FBP = filtered back projection, FIRST = forward projected model-based iterative reconstruction solution, SEMAR = single energy metal artifact reduction.

[*,†]A significant difference presents between the 2 or 3 groups.

[‡] Bonferroni-corrected *P* value.

Table 3

Nodule detection score stratified by nodule density.

Slice thickness							
	Nodule density	5mm			0.5mm		
Radiation dose		10 mA	50 mA	300 mA	10 mA	50 mA	300 mA
FBP	100 HU	3.0±2.0	4.0±1.7	3.7±0.6	2.3±1.5*	3.6±1.5	5.0±0.0
SEMAR		3.0±2.0	4.7±0.6	5.0±0.0	2.3±1.5†	4.3±0.5	5.0±0.0
FIRST		4.7±1.2	4.7±0.6	5.0±0.0	4.6±0.5*,†	5.0±0.0	5.0±0.0
P‡		.135	.368	.368	.0498	.156	1.000
FBP	−630HU	1.7±1.0	1.7±1.2	3.3±2.1	1.0±0.0	1.6±1.1	3.6±1.5
SEMAR		1.7±1.0	2.7±2.1	3.7±1.5	1.3±0.5	1.6±1.1	4.3±0.5
FIRST		2.7±1.5	4.3±1.2	4.3±1.2	3.0±2.0	4.0±1.0	4.6±0.5
P‡		.0498	.0821	.156	.156	.500	.156
FBP	−800 HU	1.0±0.0	1.0±0.0	2.7±1.5	1.0±0.0	1.0±0.0	2.0±1.0
SEMAR		1.0±0.0	1.7±1.2	3.0±2.0	1.0±0.0	1.3±0.5	3.0±1.0
FIRST		1.3±1.2	2.7±2.1	3.0±2.0	1.6±1.1	3.3±0.5	3.6±1.5
*P**		.368	.156	.368	.368	.0608	.0597

Data are presented as mean±standard deviation. The subjective image analysis on nodule detection is presented as nodule detection score (5-point scale: 1, definitely absent; 2, probably absent; 3, undeterminable; 4, probably present; 5, definitely present). FBP = filtered back projection, FIRST = forward projected model-based iterative reconstruction solution, HU = Hounsfield units,SEMAR = single energy metal artifact reduction.

‡ Bonferroni-corrected *P* value.

*,† A significant difference presents between the 2 or 3 groups.

showed the best scores under all conditions. SEMAR showed scores somewhere between those of FBP and FIRST, similar to FIRST under standard dose and closer to FBP with low doses. For nodule sizes of 10- and 5-mm, scores were better using 5-mm thickness, and with 3-mm nodules, detection scores were better with 0.5-mm thickness for all 3 methods.

3.6. Quantitative measurement of SNRs

Objective image noise on CT images of 5- and 0.5-mm slice thickness at 10 mA, 50 mA, and 300 mA is shown in Figure 4. On CT images of 5-mm slice thickness, SNR was significantly higher with FIRST than with FBP or SEMAR at low doses (10 and 50 mA), and SNRs of SEMAR and FIRST were significantly higher than that of FBP on the standard-dose CT image of 5-mm slice thickness. SNRs of SEMAR and FIRST were almost the same. On CT images of 0.5-mm slice thickness, the SNR of FIRST was significantly higher than that of FBP and SEMAR regardless of tube current.

4. Discussion

Our study showed metal artifacts were reduced the most by FIRST at low dose, and by SEMAR at standard dose. At standard dose, Yasaka et al said that SEMAR could provide images with lesser metal artefact and better depiction of structures than FIRST in neck CT, and Pan et al described that the SEMAR algorithm produced images with significantly fewer artifacts than the iterative reconstruction alone.[4,11] At low dose, Toso et al described that metal artifact reduction (MAR) algorithms improve Hounsfield units near the implant and decrease image noise in bone than iterative reconstruction.[12] This was due to the difference in the composition of the metal devices present. Although we investigated a pacemaker in this study, Pan et al[11]

Table 4

Nodule detection score stratified by nodule size.

	Nodule size	Slice thickness					
		5 mm			0.5 mm		
Radiation dose		10 mA	50 mA	300 mA	10 mA	50 mA	300 mA
FBP	10 mm	3.0±2.0	2.7±1.5	4.7±0.6	2.0±1.7	3.0±2.0	4.3±1.1
SEMAR		3.0±2.0	4.0±1.7	5.0±0.0	2.3±1.5	3.3±1.5	4.6±0.5
FIRST		3.7±1.5	5.0±0.0	5.0±0.0	4.3±1.1	4.6±0.5	5.0±0.0
*P**		.135	.156	.368	.0608	.156	.368
FBP	5 mm	1.7±1.2	2.3±2.3	4.0±1.0	1.3±0.5	2.0±1.7	3.6±1.5
SEMAR		1.7±1.2	2.7±2.1	4.0±1.0	1.3±0.5	2.0±1.7	4.0±1.0
FIRST		2.7±1.7	4.3±1.2	4.3±1.2	3.0±2.0	4.0±1.0	4.6±0.5
*P**		.135	.156	.368	.135	.0498	.156
FBP	3 mm	1.0±0.0	1.3±0.6	2.0±1.7	1.0±0.0	1.3±0.5	2.6±2.0
SEMAR		1.0±0.0	2.0±1.7	2.7±2.1	1.0±0.0	2.0±1.7	3.6±1.5
FIRST		2.0±1.0	2.7±1.5	3.0±2.0*	2.0±1.7	3.6±1.1	3.6±1.5
*P**		.135	.223	.0821	.368	.0608	.135

Data are presented as mean±standard deviation. The subjective image analysis on nodule detection is presented as nodule detection score (5-point scale: 1, definitely absent; 2, probably absent; 3, undeterminable; 4, probably present; 5, definitely present).

FBP = filtered back projection, FIRST = forward projected model-based iterative reconstruction solution, SEMAR = single energy metal artifact reduction.

* Bonferroni-corrected *P* value.

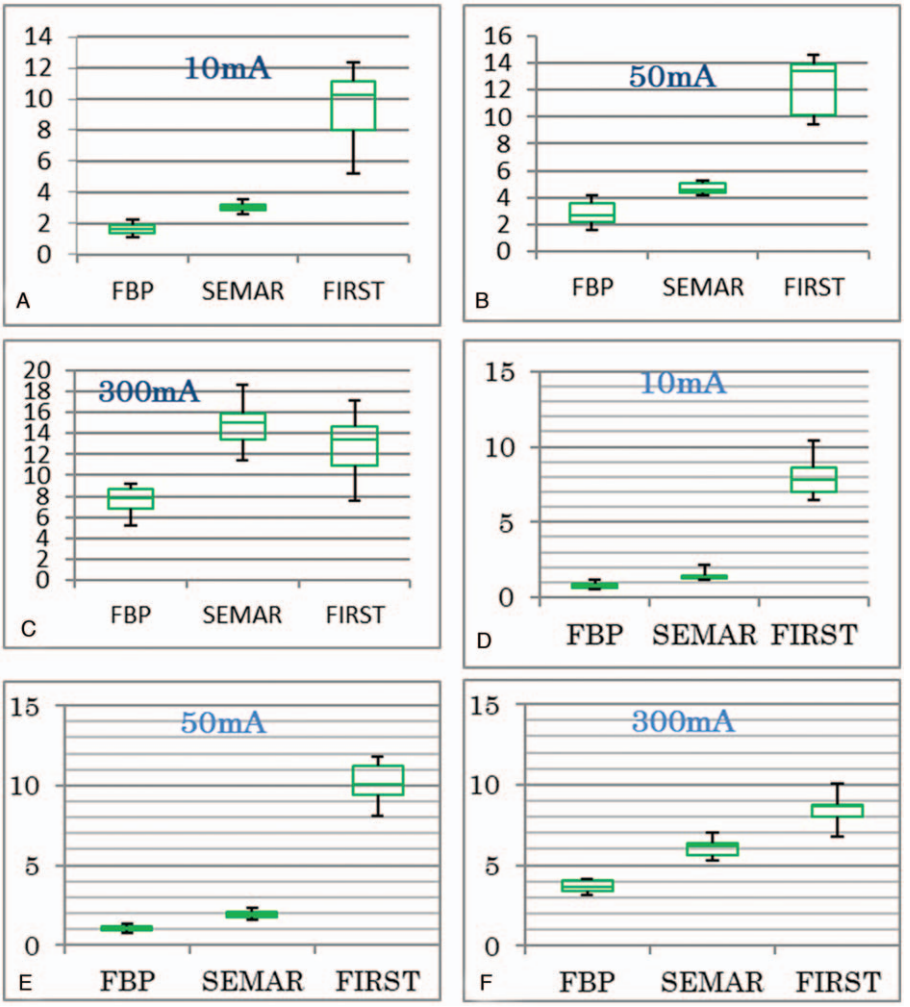

Figure 4. Quantitative measurement of SNR (mean ± standard deviation). On 5-mm thickness (A–C), 10 mA: FBP (1.7 ± 0.5), SEMAR (3.1 ± 0.3), FIRST (10.3 ± 2.8); 50 mA: FBP (2.6 ± 0.9), SEMAR (4.6 ± 0.5), FIRST (13.4 ± 2.8); 300 mA: FBP (7.8 ± 1.6), SEMAR (11.4 ± 3.2), FIRST (13.4 ± 3.6). On 0.5 mm thickness (D–F), 10 mA: FBP (0.8 ± 0.2), SEMAR (1.4 ± 0.3), FIRST (7.8 ± 1.2); 50 mA: FBP (1.0 ± 0.2), SEMAR (1.9 ± 0.2), FIRST (10.1 ± 1.3); 300 mA: FBP (3.7 ± 0.4), SEMAR (6.2 ± 0.5), FIRST (9.7 ± 0.9). FBP = filtered back projection, FIRST = forward-projected model-based iterative reconstruction solution, SEMAR = single-energy metal artifact reduction, SNR = signal-to-noise ratio.

used a cerebral aneurysm coil, Yasaka et al[4] used artificial teeth, and Toso et al[12] used orthopedic prostheses. These metal devices are usually constructed using only a single type of metal, whereas a pacemaker contains a complex structure of different types of metal and is thus considered to yield a complicated shower artifact. Therefore, at low dose with higher noise, the shower artifact is considered more difficult to eliminate. This is also supported by the worse performance with thin slice (0.5-mm), which contains more noise. However, FIRST could reduce both noise and metal artifacts without distinction, and is thus thought to be able to produce relatively clearer images when more noise is present. At standard dose with less noise, SEMAR could yield clearer images due to the specific ability to reduce metal artifacts.

When nodule detection scores were compared at low dose, FIRST performed best for all nodule sizes and/or slices. Previously, Yamada et al showed that FIRST offered better nodule detection ability than FBP, supporting our results.[13] However, no studies appear to have clarified nodule detection ability under different radiation doses between iterative reconstruction and single-energy metal artifact reduction methods. Our results concluded that FIRST performed better for nodule detection at low dose, at least under conditions of a pacemaker present. This can be attributed to the noise reduction aspect of FIRST.

When analyzed by nodule density, FIRST was able to detect nodules above -600 HU at ultra-low dose and even nodules of -800 HU at low dose. According to another experiment without any artificial objects, model-based iterative reconstruction (MBIR) was able to detect GGN of -630 HU at 20% of the standard dose, and -800 HU at 40% without any significant difference.[14] Our data support those previous results and also found that FIRST is useful even under a pacemaker at low dose. Meanwhile, SEMAR turned out to be very useful for detecting GGNs at low dose in our results.

When analyzed using nodule size, FIRST was able to detect 5-mm nodules and above at ultra-low dose, and even 3-mm nodules at low dose. Previously, Doo et al found that FIRST was helpful at low dose using 5-mm nodule volumetry without artificial

objects.[15] Our data added that FIRST could be used to detect even smaller nodules with a pacemaker present. However, it was difficult for SEMAR to detect nodules smaller than 5-mm diameter at low dose. Based on these findings, FIRST is to be recommended and preferred for nodule detection at low dose.

At standard dose, FIRST showed similar results at 50 mA, whereas SEMAR performed better when evaluated using nodule density. SEMAR could detect solid nodules just as well as FIRST and no worse for GGNs. When evaluated by nodule size, SEMAR performed just as well as FIRST at 5-mm and even 3-mm diameter. Previous research has also shown the utility of SEMAR at standard dose. Both Yasaka et al and Wellenberg et al with the presence of artificial teeth and artificial joints, respectively, found better results with SEMAR than with FIRST at standard dose.[4,16] Although our data have slightly different results, we can conclude that at standard dose, SEMAR is warranted for nodule detection even in patients with a pacemaker. One advantage of using SEMAR is the relatively short scan time compared with FIRST. SEMAR can take 70 images/s, FIRST takes about 1.8 images/s. Overall, in terms of using standard dose, SEMAR is better suited even with a pacemaker present.

SEMAR always showed better nodule detection score with thin slices than with thick slices, regardless of the nodule size. This result confirms previous research by Schaller et al with iterative reconstruction.[17] This may be attributed to the noise-reduction ability of iterative reconstruction counterbalancing the noise created with a thin slice, resulting in higher spatial resolution.

Our research has some limitations. We only used a chest phantom and simulated nodules in our study to evaluate nodule detection. Normally with the human body, tissues are more complex and body movements would reduce image clarity. We analyzed using an ideal, uniform, motionless setting, not matching actual clinical situations. Our sample size was also a limitation. Nodule types and conditions can show different values with even small changes.

In conclusion, FIRST showed better nodule detection ability at low dose, even with a pacemaker present, and SEMAR offers comparable detection to FIRST at standard dose, but with shorter scan times. Certain methods of scanning and reconstructions are being identified as preferable according to the specific clinical setting and artificial materials present in the patient. Moreover, the latest CT device (Aquilion Precision; Canon Medical Systems) can provide images reconstructed using both FIRST and SEMAR at the same time. Further analyses for nodule detectability are needed in clinical settings.

Author contributions

Conceptualization: Noriko Kikuchi, Masahiro Yanagawa, Noriyuki Tomiyama.
Data curation: Noriko Kikuchi, Masahiro Yanagawa, Yukihiro Enchi, Yuriko Yoshida, Tomo Miyata.
Formal analysis: Noriko Kikuchi, Masahiro Yanagawa.
Investigation: Noriko Kikuchi, Masahiro Yanagawa, Yukihiro Enchi, Akiko Nakayama, Akinori Hata, Yuriko Yoshida, Tomo Miyata.
Methodology: Noriko Kikuchi, Masahiro Yanagawa, Akinori Hata.
Supervision: Masahiro Yanagawa, Osamu Honda, Noriyuki Tomiyama.
Writing – original draft: Noriko Kikuchi.
Writing – review & editing: Masahiro Yanagawa, Mitsuko Tsubamoto, Noriyuki Tomiyama.

References

[1] Boas FE, Fleischmann D. Evaluation of two iterative techniques for reducing metal artifacts in computed tomography. Radiology 2011;259:894–902.
[2] Boas FE, Fleischmann D. CT artifacts: causes and reduction techniques. Imag Med 2012;4:229–40.
[3] Stadiotti P, Curti A, Castellazzi G, et al. Metal-related artifacts in instrumented spine. Techniques for reducing artifacts in CT and MRI: state of the art. Eur Spine J 2009;18:102–8.
[4] Yasaka K, Kamiya K, Irie R, et al. Metal artefact reduction for patients with metallic dental fillings in helical neck computed tomography: comparison of adaptive iterative dose reduction 3D (AIDR 3D), forward-projected model-based iterative reconstruction solution (FIRST) and AIDR 3D with single-energy metal artefact reduction (SEMAR). Dentomaxillofac Radiol 2016;45:7.
[5] Tatsugami F, Higaki T, Sakane H, et al. Coronary CT angiography in patients with implanted cardiac devices: initial experience with the metal artefact reduction technique. Br J Radiol 2016;89:1067.
[6] Miki K, Mori S, Hasegawa A, et al. Single-energy metal artefact reduction with CT for carbon-ion radiation therapy treatment planning. Br J Radiol June 2016;89:1062.
[7] Shirota G, Maeda E, Namiki Y, et al. Pediatric 320-row cardiac computed tomography using electrocardiogram-gated model-based full iterative reconstruction. Pediatric Radiol 2017;47:1463–70.
[8] Maeda E, Tomizawa N, Kanno S, et al. The feasibility of Forward projected model-based Iterative Reconstruction SoluTion (FIRST) for coronary 320-row computed tomography angiography: a pilot study. J Cardiovasc Comput Tomogr 2017;11:40–5.
[9] Nishiyama Y, Tada K, Nishiyama Y, et al. Effect of the forward-projected model-based iterative reconstruction solution algorithm on image quality and radiation dose in pediatric cardiac computed tomography. Pediatr Radiol 2016;46:1663–70.
[10] American Association of Physicists in Medicine. The measurement, reporting, and management of radiation dose in CT; 2008. Available at: http://www.aapm.org/pubs/reports/rpt_96.pdf. Accessed January 15, 2012.
[11] Pan YN, Chen G, Li AJ. Reduction of metallic artifacts of the post-treatment intracranial aneurysms: effects of single energy metal artifact reduction algorithm. Clin Neuroradiol 2019;29:277–84.
[12] Toso S, Laurent M, Lozeron ED, et al. Iterative algorithms for metal artifact reduction in children with orthopedic prostheses: preliminary results. Pediatr Radiol 2018;48:1884–90.
[13] Yamada Y, Jinzaki M, Tanami Y, et al. Model-based iterative reconstruction technique for ultralow-dose computed tomography of the lung: a pilot study. Invest Radiol 2012;47:482–9.
[14] Kelsey B, Hua Ai , Fox PS, et al. Radiation dose reduction for CT lung cancer screening using ASIR and MBIR: a phantom study. J Appl Clin Med Phys 2014;15:271–80.
[15] Doo KW, Kang EY, Yang HS, et al. Accuracy of lung nodule volumetry in low dose CT with iterative reconstruztion: an anthropomorphic thoracic phantom study. Br J Radiol 2014;87:1041.
[16] Wellenberg RH, Boomsma MF. Low-dose CT imaging of a total hip arthroplasty phantom using model-based iterative reconstruction and orthopedic metal artifact reduction. Skeletal Radiol 2017;46:623–32.
[17] Schaller F, Sedlmair M, Raupach R, et al. Noise reduction in abdominal computed tomography applying iterative reconstruction (ADMIRE). Acad Radiol Oct 2016;23:1230–8.